Journal of Science and Technology in Civil Engineering, HUCE (NUCE), 2022, 16 (3): 84–96

PREDICTING TENSILE PROPERTIES OF STRAIN-HARDENING CONCRETES CONTAINING HYBRID FIBERS FROM SINGLE FIBER PULLOUT RESISTANCE

Duy-Liem Nguyen[a], Tri-Thuong Ngo[b,*], Tan-Duy Phan[a], Thanh-Tu Lai[a], Duc-Viet Le[a]

[a]*Faculty of Civil Engineering, Ho Chi Minh City University of Technology and Education, 01 Vo Van Ngan street, Thu Duc city, Ho Chi Minh city, Vietnam*
[b]*Faculty of Civil Engineering, Thuyloi University, 175 Tay Son street, Dong Da district, Ha Noi, Vietnam*

Article history:
Received 24/3/2022, Revised 10/5/2022, Accepted 23/5/2022

Abstract

Tensile properties of strain-hardening fiber-reinforced concrete are the key engineering parameters in determining bending resistance of the material. In this paper, an analytical model to predict tensile properties of ultra-high-performance fiber-reinforced concrete (UHPFRC), a type of strain-hardening fiber-reinforced concretes, was performed based on single fiber pullout test. The studied UHPFRCs contained hybrid fiber system, including macro steel fiber combined with micro steel fiber. Three types of macro steel fibers were used, including long smooth fiber (LS), hooked A fiber (HA), and hooked B fiber (HB); they had different lengths and geometries but same volume content (1.0 %). The only short smooth fiber (SS), one type of micro steel fiber, was employed with various volume content (0.5 %, 1.0 %, 1.5 %). The experimental data from the fiber pullout tests in the available references were used to predict the first crack/post crack strength and cracking parameters of UHPFRCs with hybrid fibers. The predictive equations for strengths and crack resistance of UHPFRC containing hybrid fibers were proposed with modified coefficients.

Keywords: UHPFRC; first cracking; post cracking; hybrid fiber; micro cracks.

https://doi.org/10.31814/stce.huce(nuce)2022-16(3)-07

1. Introduction

There is always an increasing demand for enhancing mechanical resistance and durability of civil/military constructions owing to risk of wars or natural disasters. Ultra-high-performance fiber-reinforced concretes (UHPFRCs) or high-performance fiber- reinforced concretes (HPFRCs) is very suitable for the target of enhancing the strength, ductility, toughness, and durability of constructions. For instance, due to highly densified microstructure, UHPFRCs could produce compressive strength more than 150 MPa [1], uniaxial tensile and flexural strength up to 10 MPa and 30 MPa, respectively [2, 3]. Furthermore, UHPFRCs could produce work-hardening response with an increase of load after the first crack under tension/flexure [4–6]. This property is due to stress bridging of discrete fibers across micro cracks of the tested specimens, and results in large ductility, large energy absorption

*Corresponding author. *E-mail address:* trithuong@tlu.edu.vn (Ngo, T.-T.)

capacity, and high cracking resistance of UHPFRCs. Based on superior mechanical properties highlighted above, UHPFRC/HPFRC could be applied in long-span bridges, high-rise buildings with many benefits [7, 8]. The work-hardening or work-softening behavior of UHPFRC/HPFRC depends much on the features of fibers embedded in its matrix [9, 10]. Fiber type, geometry, aspect ratio, volume fraction, orientation, and distribution in UHPFRC/HPFRC matrix were reported as considerable factors influencing mechanical parameters of UHPFRC/HPFRC [3, 11–13].

According to some available guidelines for UHPFRC/HPFRC, the mechanical properties of UHPFRC/HPFRC was correlated to fiber-matrix bond strength measured from fiber pullout test [14, 15]. The pullout behaviors of steel fiber were highly influenced by characteristics of matrix and fiber, which mainly govern the cohesive interfacial bonding between them [16]. The distribution and content of fibers mixed in matrix also affected the mechanical properties of the concretes [4, 17]. Lately, several studies have reported that there were synergy behaviors in employing the hybrid steel fiber system in UHPFRC/HPFRC under static/high strain rate loads. For example, there were the improved mechanical resistances of UHPFRC/HPFRC using hybrid fibers in comparison with those using mono macro or micro fibers with same fiber content in tension [18, 19], flexure [20] or shear [21]. The observations can be referred to optimize the fiber content used in UHPFRC/HPFRC and consequently minimize the cost of UHPFRC/HPFRC.

Nonetheless, the correlation between fiber pullout performance and tensile/flexural properties of UHPFRCs employing hybrid fibers has been still lacking. This is really an issue for practical application of UHPFRC/HPFRC in designing work. This situation has motivated the authors to conduct the analytical study focusing on tensile parameters of UHPFRCs using steel hybrid macro/micro fibers. Based on the tensile parameters of UHPFRCs, flexural resistance of UHPFRCs could also be estimated. It is expected that the utilization of UHPFRC/HPFRC with hybrid fibers will be conveniently and properly applied.

2. Relationship between strain hardening tensile behavior of UHPFRC and pullout mechanism of single fiber type

The reinforcing fibers, with suitable type and volume fraction into plain UHPFRC, can produce strain-hardening tensile behaviors of UHPFRCs. Fig. 1 displays a typical tensile stress versus strain behavior of UHPFRC. As can be seen in Fig. 1, two key points describing the direct tensile behavior are identified in the stress versus strain curve: the first-cracking point ($\varepsilon_{cc}, \sigma_{cc}$) and the post-cracking point ($\varepsilon_{pc}, \sigma_{pc}$). The first-cracking point is defined as the limit of the linear elastic region while the post-cracking point is defined as the point where the maximum stress occurs and the crack-opening region starts [22]. The first-cracking and the post-cracking point in this figure were key points characterizing strain-hardening of UHPFRC with condition of $\sigma_{pc} > \sigma_{cc}$ [22]. Typically, the characteristic strain-hardening of UHPFRC is three stages including elastic before the first-crack (OA), hardening behavior from first - crack to the post-crack (AB), and softening behavior (BC) after the post-crack.

According to references [15, 23, 24], the post-crack strength is directly dependent on the bond strength at the interface between fiber and matrix. Assuming that the bond strength is a constant over the entire embedment length, the equivalent bond strength (τ_{eq}) can be computed from the pullout work ($E_{pullout}$), which obtained from a single fiber pullout test. If the equivalent bond strain is a constant, the pullout load versus slip respond curves will be triangular, as described in Fig. 2. Using the pullout work, the equivalent bond strength for a typical fiber can be expressed using Eq. (1). Based on the strain-hardening tensile behaviors of UHPFRCs and single fiber pullout test, the first-cracking strength (σ_{cc}) and post-cracking strength (σ_{pc}) can be calculated using Eqs. (2) and (3), respectively

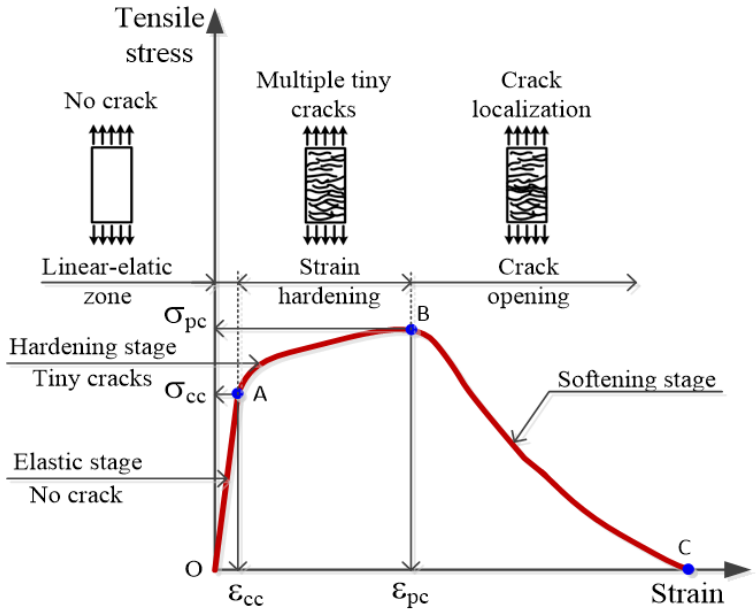

Figure 1. Tensile behavior of UHPFRC with tensile parameters [15]

[15] while the theoretical number of fibers within cross section (N_f) and the average crack spacing (ΔL_{av}) can be given using Eqs. (4) and (5), respectively [23, 24]. The number of tiny cracks (N_{cr}) within gauge length of specimen can be computed using Eq. (6).

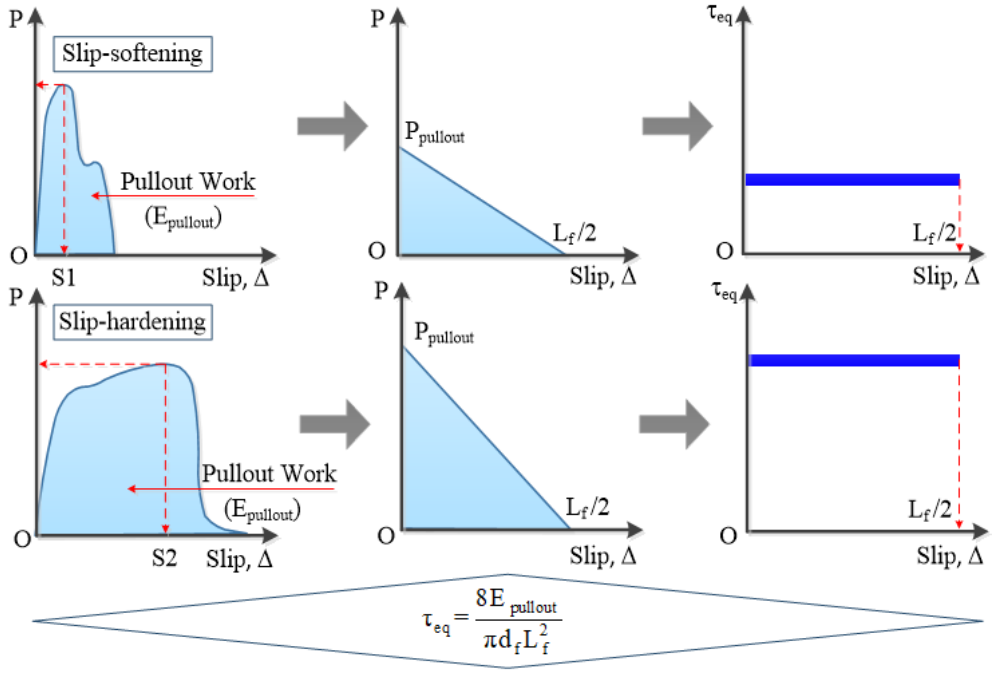

Figure 2. Determination of equivalent bond strength at the interface between fiber and matrix

$$E_{pullout} = \frac{1}{2}P_{pullout} \times \left(\frac{L_f}{2}\right) = \frac{1}{2}\pi d_f \tau_{eq} \times \left(\frac{L_f}{2}\right) \times \left(\frac{L_f}{2}\right) \rightarrow \tau_{eq} = \frac{8E_{pullout}}{\pi d_f L_f^2} \tag{1}$$

$$\sigma_{cc} = E_{cc}\varepsilon_{cc} = [E_m(1 - V_f) + E_f V_f]\frac{\sigma_m}{E_m} = [(1 - V_f) + \frac{E_f}{E_m}V_f]\sigma_m \tag{2}$$

$$\sigma_{pc} = \alpha_2 \tau_{eq}\frac{L_f}{d_f}V_f \tag{3}$$

$$N_f = \alpha_2 \frac{V_f}{a_f}A_g \tag{4}$$

$$\Delta L_{av} = \eta \frac{A_m \sigma_m}{(N_f \pi d_f)\tau_{eq}} \tag{5}$$

$$N_{cr} = \frac{L}{\Delta L_{av}} \tag{6}$$

where, E_{cc}, E_f, and E_m are the elastic modulus of composite, fiber and matrix, respectively; d_f and L_f are the diameter and length of fiber; V_f is the fiber volume fraction; A_m and σ_m are area and tensile strength of matrix, respectively; α_2 is coefficient considering the orientation of fibers, its value is 1, $2/\pi$, and 0.5 for the case of 1, 2 and 3D fiber orientation, respectively. $A_g$is cross section area of tensile specimen. λ_1 is coefficient for considering average pullout length ratio, orientation effect and group reduction. $a_f = \dfrac{\pi d_f^2}{4}$ is sectional area of one fiber; L is gauge length of tensile specimen. And, η is crack spacing factor, its value ranging from 1 to 2. The value of η is 1.5 for no experimental observation. In addition, k_1, k_2, k_3 are modified coefficients considering group fiber effect, pullout length ratio of fiber [15], different compositions of plain concretes, different experimental conditions...

3. Proposed models and equations for tensile parameters of UHPFRCs using hybrid fibers

Under direct tension, an axial loading P applied to the hybrid fibers of tensile specimens at an any section, as shown in Fig. 3. Considering of P value is first assumed to can create stresses in the matrix smaller than its tensile strength, i.e., no cracking occurs. Due to symmetry property, only half of the section is considered for analysis. The distance of any section along the tensile specimen was defined by its horizontal line x from the left section ($x \leq L/2$). The load is transmitted from hybrid fibers to the matrix over a certain distance and strain in the fiber becomes equivalent one in the matrix.

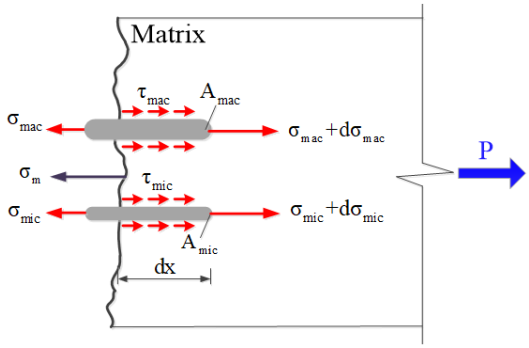

Figure 3. Hybrid fibers bridging crack with pullout mechanism

Prior to any cracking happens, from equilibrium conditions of the forces, we had:

$$P = P_{mac} + P_{mic} + P_m \tag{7}$$

For a given P with condition of $dP = 0$, Eq. (7) could be written as follows:

$$A_{mac}d\sigma_{mac} + A_{mic}d\sigma_{mic} = -A_m d\sigma_m \tag{8}$$

From equilibrium conditions of an infinitesimal fiber element, d_x, as can be seen from Fig. 3, we had:

$$\begin{aligned} &A_{mac}\left[\sigma_{mac} - (\sigma_{mac} - d\sigma_{mac})\right] + A_{mic}\left[\sigma_{mic} - (\sigma_{mic} - d\sigma_{mic})\right] = \rho_{mac}\tau_{mac}dx + p_{mic}\tau_{mic}dx \\ &\Leftrightarrow A_{mac}d\sigma_{mac} + A_{mic}d\sigma_{mic} = \rho_{mac}\tau_{mac}dx + p_{mic}\tau_{mic}dx \end{aligned} \tag{9}$$

In Eq. (9), where ρ_{mac} and ρ_{mac} are represent the perimeter of macro and micro fiber, respectively. Next, using integration method, Eq. (9) becomes Eq. (10) as follows:

$$A_{mac}\sigma_{mac} + A_{mic}\sigma_{mic} + C = (\rho_{mac}\tau_{mac} + \rho_{mic}\tau_{mic})x \tag{10}$$

In Eq. (10), where C is a constant, which is obtained from appropriated boundary conditions. For $x = 0$, the force in fiber is equivalent to the applied load P. Hence, we had:

$$\begin{cases} A_{mac}\sigma_{mac} + A_{mic}\sigma_{mic} + C = 0 \\ A_{mac}\sigma_{mac} + A_{mic}\sigma_{mic} = P \end{cases} \Leftrightarrow C + P = 0 \tag{11}$$

Substituting C from Eq. (11) together with Pvalue from Eq. (7) into Eq. (10), the value of $x$can be drawn as follows:

$$x = \frac{\sigma_m A_m}{\rho_{mac}\tau_{mac} + \rho_{mic}\tau_{mic}} \tag{12}$$

As the stress in the matrix reaches its ultimate strength, the first cracking occurs, i.e., $\sigma_m = \sigma_{mu}$. The shortest distance, at which the first cracking occurs, will relate to the x value with $\sigma_m = \sigma_{mu}$. Therefore, this shortest distance ($\Delta L_{\min}$) also represents the smallest crack spacing or distance between two cracks, as described in Fig. 4. The value of $\Delta L_{\min}$ is obtained from Eq. (12), in which σ_m is substitute by σ_{mu}, as given in Eq. (13). According to Fig. 4, it can be seen that the maximum distance between two cracks will relate to triangular stress profiles leading to the $\Delta L_{\max} = 2\Delta L_{\min}$ [22, 25]. Because cracks happen randomly, the spacing (ΔL) between any two consecutive cracks such as points A and C in Fig. 4 can be computed using Eq. (14). The average crack spacing (ΔL_{av}) can be estimated using Eq. (15). In this equation, η is from 1 to 2, corresponding to the range between minimum and maximum crack spacing.

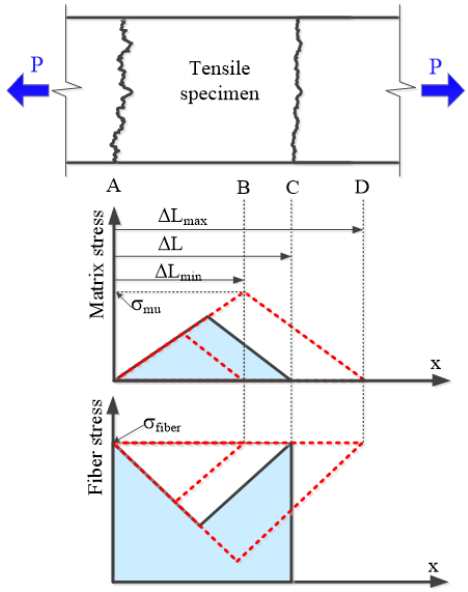

Figure 4. Demonstration of minimum and maximum theoretical crack spacing

$$\Delta L_{\min} = \frac{\sigma_{mu}A_m}{\rho_{mac}\tau_{mac} + \rho_{mic}\tau_{mic}} \tag{13}$$

$$\Delta L_{\min} \le \Delta L \le \Delta L_{\max} \tag{14}$$

$$\Delta L_{av} = \eta \frac{\sigma_{mu} A_m}{\rho_{mac} \tau_{mac} + \rho_{mic} \tau_{mic}} \tag{15}$$

Finally, the ΔL_{av} for due to hybrid fiber system for total the number of fiber in tensile specimen was established using in Eq. (16).

$$\Delta L_{av} = \eta \frac{A_m \sigma_{mu}}{(N_{mac} \pi d_{mac}) \tau_{mac} + (N_{mic} \pi d_{mic}) \tau_{mic}} \tag{16}$$

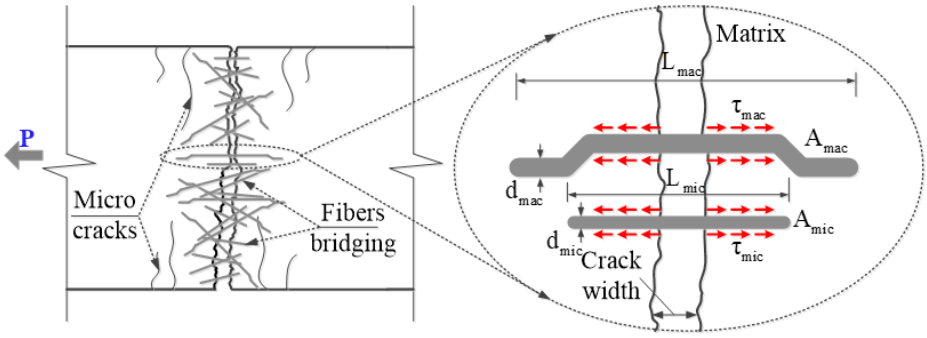

Figure 5. Stresses in matrix and hybrid fibers at an any section

A proposed model was performed in Fig. 5 for the target of forecasting the tensile parameters of UHPFRCs using hybrid fibers. The tensile parameters of UHPFRCs, including the σ_{cc} and σ_{pc} together with N_f and N_{cr} with hybrid fibers distributed randomly can be computed from Eq. (17) to Eq. (21), respectively. In each equation, V_{mac}, a_{mac}, L_{mac} and d_{mac} are represent the volume content, section area, length, and diameter of macro fiber, respectively, while V_{mic}, a_{mic}, L_{mic}, and d_{mic} are those of micro fiber, respectively. The τ_{mac} and τ_{mic} are the interfacial bond strength between the fiber and matrix of macro fiber and micro fiber, respectively, as observed in Fig. 3. The α, λ, k_1, k_2, and k_3 were defined in the previous section.

$$\sigma_{cc} = k_1 [(1 - V_{mac} - V_{mic}) + \frac{E_{mac}}{E_m} V_{mac} + \frac{E_{mic}}{E_m} V_{mic}] \sigma_m \tag{17}$$

$$\sigma_{pc} = k_2 \alpha_2 \left(\tau_{mac} \frac{L_{mac}}{d_{mac}} V_{mac} + \tau_{mic} \frac{L_{mic}}{d_{mic}} V_{mic} \right) \tag{18}$$

$$N_f = N_{mac} + N_{mic} = \alpha_2 \frac{V_{mac}}{a_{mac}} A_g + \alpha_2 \frac{V_{mic}}{a_{mic}} A_g = \alpha_2 \left(\frac{V_{mac}}{a_{mac}} + \frac{V_{mic}}{a_{mic}} \right) A_g \tag{19}$$

$$\Delta L_{av} = k_3 \eta \frac{A_m \sigma_{mu}}{(N_{mac} \pi d_{mac}) \tau_{mac} + (N_{mic} \pi d_{mic}) \tau_{mic}} \tag{20}$$

$$N_{cr} = \frac{L}{\Delta L_{av}} = \frac{L}{k_3 \eta} \frac{(N_{mac} \pi d_{mac}) \tau_{mac} + (N_{mic} \pi d_{mic}) \tau_{mic}}{A_m \sigma_{mu}} \tag{21}$$

4. Experimental program

4.1. Materials and specimen preparation

For predicting the tensile properties using equivalent bond strength of fiber from fiber pullout test, the used references were carefully chosen with approximate matrix strengths. Fig. 6 shows the

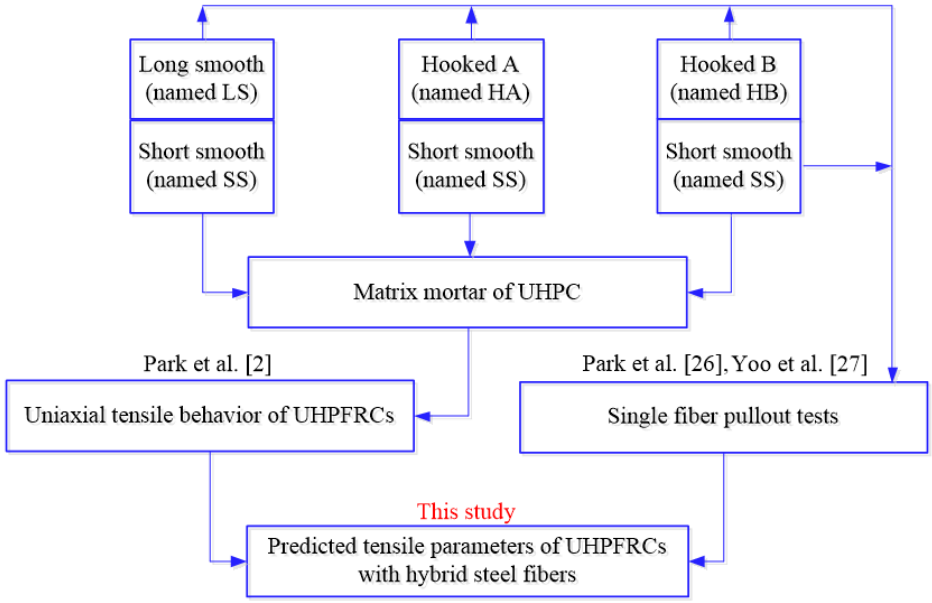

Figure 6. Flowchart of this investigation

flowchart of this investigation based on several previous studies reported by Park et al. [2], Park et al. [26], and Yoo et al. [27]). The uniaxial tensile test was performed with hybrid steel fiber and UHP matrix strengths of 200 MPa [2]. The single fiber pullout tests were used the UHP matrix strengths of 200 MPa [26] and 190 MPa [27]. It was noted that the fibers used in [2, 26], and [27]) were identical for each type with same size. In uniaxial tensile test [2], the matrix mortar of UHPC was embedded a hybrid fiber system: macro-fiber and micro fiber. The four macro fiber types were used, including long smooth fiber (LS), hooked A fiber (HA), and hooked B fiber (HB) with the same volume content of 1.0%. The micro fiber only one type was short smooth fiber (SS) with various volume content of 0.5%, 1.0%, and 1.5%. Table 1 provides 5 tensile test series which were considered from three

Table 1. Test series [2]

Macro fiber types (Volume content 1.0%)	Micro fiber volume content (%)	Notation
	Short smooth (SS)	
Long smooth (LS)	0.5	LS10SS05
	1.0	LS10SS10
	1.5	LS10SS15
Hooked A (HA)	0.5	HA10SS05
	1.0	HA10SS10
	1.5	HA10SS15
Hooked B (HB)	0.5	HB10SS05
	1.0	HB10SS10
	1.5	HB10SS15

type of macro fibers and three volume contents of micro fiber. For instance, the tensile specimen incorporating 1.0% LS and 0.5% SS is designed as LS10SS05. In single fiber pullout tests [26, 27], four types of steel fiber were investigated as follows: LS, HA, HB, and SS. The main approach of this study, forecasting tensile parameters of UHPFRC using hybrid steel fiber and those parameters were compared with testing result of Park et al. [2]. The matrix composition and compressive strength of UHPC matrix mortar were summarized in Table 2 while photos of the fiber types were displayed in Fig. 7 and their properties provided in Table 3. In Table 2, the compressive strength of UHPC was 200 MPa. The particle sizes of the silica sand used in the matrix was 500 μm while those of the silica fume was 1 μm. As shown in Table 3, the cross sections of LS, HA, HB, and SS were circular. The diameter of LS, HA, HB, and SS were 0.3 mm, 0.375 mm, 0.775 mm, and 0.2 mm while their length were 30 mm, 30 mm, 62 mm, and 13 mm, respectively. The density and elastic modulus of all steel

Table 2. Composition and compressive strength of UHPFRC used [2]

Cement	Silica Fume	Silica sand	Fly ash	Silica powder	Superplasticizer	Water	Compressive strength (MPa)
1.00	0.25	1.10	0.20	0.30	0.067	0.2	200

Table 3. Features of the fibers used in this study [2, 26, 27]

Fiber Type	Notation	Diameter (mm)	Length (mm)	Density (g/cm^3)	Aspect ratio (L/D)	Equivalent bond strength (MPa)	Tensile strength (MPa)
Long smooth	LS	0.3	30	7.9	100	9.5 [26]	2580
Hooked A	HA	0.375	30	7.9	80	7.5 [26]	2311
Hooked B	HB	0.775	62	7.9	80	7.2 [26]	1891
Short smooth	SS	0.2	13	7.9	65	9.6 [27]	2788

Note: Except for equivalent bond strength, other features of fibers were referred to [2].

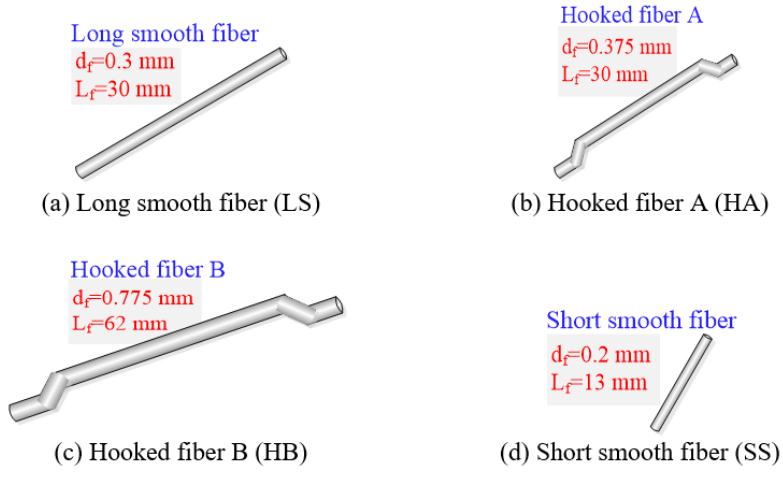

(a) Long smooth fiber (LS) (b) Hooked fiber A (HA)

(c) Hooked fiber B (HB) (d) Short smooth fiber (SS)

Figure 7. Illustrated shape of fiber types used [2]

fiber were 7.9 g/cm^3 and 200 GPa, respectively. The equivalent bond strength of all steel fiber types was obtained from single fiber pullout test, as provided in Table 2. As shown in Table 3, the equivalent bond strength of LS, HA, and HB fiber was 9.5, 7.5, and 7.2 MPa, respectively [26]. The equivalent bond strength of SS fiber was 9.61 MPa [27]. Detailed information on mixing materials of UHPFRCs and casting tensile specimens can be found in the published document [2].

4.2. Experiment setup and loading procedure

The experiment setup and testing process for uniaxial tension described in this section were referred to [2]. At least three tensile specimens per each series were tested using a universal testing machine Schmadzu AG-300 KNX. The Schmadzu AG-300 KNX operation with displacement control was applied for tensile test under loading speed of 0.4 mm/min for all specimens. The data acquisition frequency was 1 Hz. The geometry of specimen and test setup for the direct tensile test was displayed in Fig. 8(a). As shown in Fig. 8(a), the cross section of specimen was rectangular-shaped with dimension of 50×100 (width × depth) and their gauge length was 175 mm. To avoid the failure of specimens

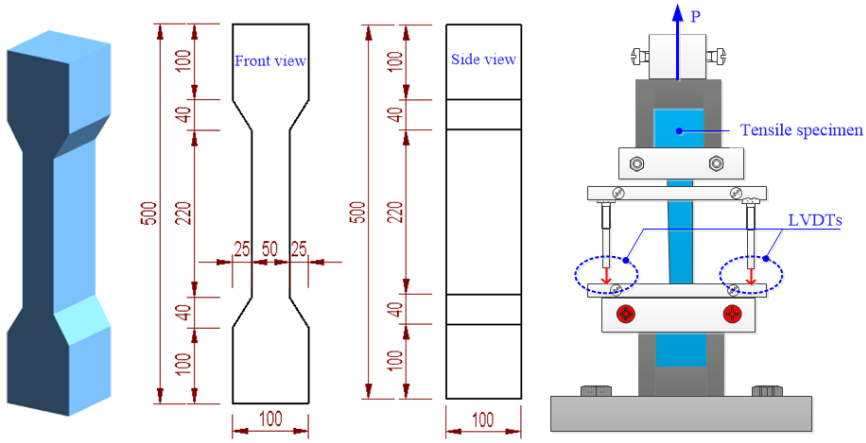

(a) Geometry and test setup for uniaxial tension [2]

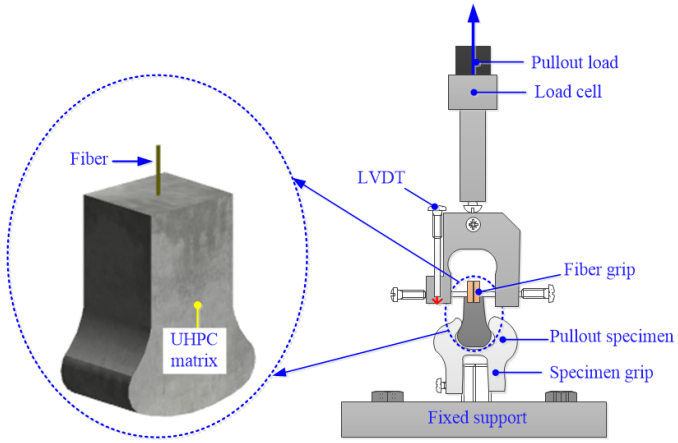

(b) Pullout test specimen and setup [26, 27]

Figure 8. Test setup for uniaxial tension and fiber pullout test

out of gauge length, the steel wire mesh was reinforced at the ends of the specimens. During the test, the load signal was measured from a load cell, which attached to the bottom of the cross head. The elongation history of the specimen was obtained from two linear variable transformers (LVDTs) attached to the frame, as described in Fig. 8. Prior to testing, all specimens were carefully aligned to avoid any influence of eccentricity on the obtained tensile response of the specimens.

The test setup and procedure for single fiber pullout test described in this section were referred to [26, 27]. Half dog-bone shaped pullout specimens were designed and tested to investigate the bond strength between matrix and steel fiber, as displayed in Fig. 8(b). The pullout load was measured from a load cell, which was attached to the top of grip for holding the fiber. The fiber slip was measured from the vertical displacement of the fiber grip using LVDT. The electromechanical universal testing machines (UTMs) used for the pullout test had a capacity of 500 kN for LS, HA, ans HB fiber [26], and 250 kN for SS fiber [27]. The speed of machine with displacement control was 1.0 mm/min.

4.3. Summarized experimental data from the tensile test in the previous study [2]

The average parameter values, including first cracking strength (σ_{cc}), post cracking strength (σ_{pc}), number of cracks (N_{cr}), and average crack spacing (ΔL_{av}) in tension of UHPFRC using hybrid fibers, were summarized and presented in Table 4. As shown in Table 4, the highest value of σ_{cc} was 11.35 MPa for tensile specimen using HB fiber (1.0%) combined with SS fiber (0.5%). The highest value of σ_{pc} was 13.84 MPa for tensile specimen using HA fiber (1.0%) combined with SS fiber (1.5%). The N_{cr} value for all tensile specimens ranged from 4.67 to 39.00 while the value of ΔL_{av} changed between 4.50 and 38.89 mm. It was highlighted that the number of cracks visibly increased as the volume content of SS fiber increased from 0.5% up to 1.5%. The tensile parameters were enhanced due to the addition of SS fiber to form a system of hybrid fibers, which strongly affected both strain hardening and multiple micro cracking behavior of UHPFRCs [2].

Table 4. Experimental tensile parameters of UHPFRC using hybrid fibers [2]

Specimen series	First cracking, σ_{cc} (MPa)	Post cracking, σ_{pc} (MPa)	Number of cracks N_{cr} (ea)	Average crack spacing ΔL_{av} (mm)
LS10SS05	9.14	11.42	4.67	38.89
LS10SS10	9.62	13.31	15.33	12.13
LS10SS15	9.88	13.22	26.67	6.66
HA10SS05	10.75	10.90	6.00	30.63
HA10SS10	10.06	12.25	27.00	6.56
HA10SS15	10.52	13.84	34.00	5.15
HB10SS05	11.35	10.31	21.50	8.67
HB10SS10	9.14	11.33	31.33	5.60
HB10SS15	10.65	12.01	39.00	4.50

5. Derivation of modified coefficients in the equations to predict tensile parameters of UHPFRC using hybrid fibers

The equations to predict the σ_{cc}, σ_{pc}, ΔL_{av}, and N_{cr} were given in Eqs. (17), (18), (20), and (21), respectively. Based on the experimental data presented in Table 4, the modified coefficients were derived and provided in Table 5. As shown in Table 5, the ranges of the modified coefficients were as

follows: k_1 from 1.58 to 2.26 for σ_{cc}, k_2 from 1.23 to 2.10 for σ_{pc}, and k_3 from 1.42 to 4.76 for ΔL_{av} and N_{cr}. It was noticed that the first value of k_3 was not considered due to significant difference. The average values of k_1, k_2, and k_3 were 1.81, 1.65 and 3.02, respectively.

Table 5. Modified coefficients in predictive equations of tensile parameters

Specimen series	First cracking, σ_{cc} (MPa)	Post cracking, σ_{pc} (MPa)	Average crack spacing ΔL_{av} (mm)
	Coefficient k_1	Coefficient k_2	Coefficient k_3
LS10SS05	1.82	1.59	10.61 (omitted)
LS10SS10	1.71	1.49	4.76
LS10SS15	1.58	1.23	3.42
HA10SS05	2.14	2.10	6.61
HA10SS10	1.78	1.76	2.20
HA10SS15	1.68	1.58	2.35
HB10SS05	2.26	2.04	1.42
HB10SS10	1.62	1.66	1.58
HB10SS15	1.70	1.40	1.81
Average	1.81	1.65	3.02

6. Conclusions

The study work provided helpful information about theoretical model to predict tensile parameters of UHPFRCs using hybrid fibers based on experimental results from several published documents. Based on the analytical study, the following specific conclusions can be drawn from the study described herein:

- The experimental data from single fiber pullout test can be used to predict first crack/post crack strength and cracking parameters of UHPFRCs using hybrid fibers. However, the predicted values are observed to be much lower than the experimental values.

- Based on the experimental data, the average modified coefficients for the first crack strength, post crack strength, and cracking parameters of UHPFRCs were 1.81, 1.65 and 3.02 in the predictive equations, respectively.

- The analytical model and equations suggested in this study can be a potential tool for predicting tensile parameters of UHPFRCs using hybrid fibers. It is helpful for structural designer saving time and cost.

Acknowledgements

This work belongs to the project Grant No. B2021-SPK-08 funded by Ministry of Education and Training, and hosted by Ho Chi Minh City University of Technology and Education, Vietnam.

References

[1] Graybeal, B. A. (2007). Compressive behavior of ultra-high-performance fiber-reinforced concrete. *ACI Materials Journal*, 104(2):146–152.

[2] Park, S. H., Kim, D. J., Ryu, G. S., Koh, K. T. (2012). Tensile behavior of Ultra High Performance Hybrid Fiber Reinforced Concrete. *Cement and Concrete Composites*, 34(2):172–184.

[3] Kim, D. J., Park, S. H., Ryu, G. S., Koh, K. T. (2011). Comparative flexural behavior of Hybrid Ultra High Performance Fiber Reinforced Concrete with different macro fibers. *Construction and Building Materials*, 25(11):4144–4155.

[4] Song, J., Nguyen, D. L., Manathamsombat, C., KIM, D. J. (2015). Effect of fiber volume content on electromechanical behavior of strain-hardening steel-fiber-reinforced cementitious composites. *Journal of Composite Materials*, 49(29):3621–3634.

[5] Kim, M. K., Kim, D. J., An, Y.-K. (2018). Electro-mechanical self-sensing response of ultra-high-performance fiber-reinforced concrete in tension. *Composites Part B: Engineering*, 134:254–264.

[6] Kim, D., Kang, S., Ahn, T.-H. (2014). Mechanical Characterization of High-Performance Steel-Fiber Reinforced Cement Composites with Self-Healing Effect. *Materials*, 7(1):508–526.

[7] Chung, D. D. L. (2004). Electrically conductive cement-based materials. *Advances in Cement Research*, 16(4):167–176.

[8] Schmidt, M., Fehling, E. (2005). Ultra-high-performance concrete: research, development and application in Europe. In *Proceeding of 7th International Symposium on the Utilization of High-Strength and High-Performance Concrete, ACI Washington, SP*, volume 228, 51–78.

[9] Empelmann, M., Teutsch, M., Steven, G. (2008). Improvement of the post fracture behaviour of UHPC by fibres. In *Proceeding of 2nd International Symposium on Ultra High Performance Concrete, March, Kassel University press GmbH, Kassel*, 177–184.

[10] Song, J., Nguyen, D. L., Manathamsombat, C., Dong Joo, K. I. M. (2015). Effect of fiber volume content on electromechanical behavior of strain-hardening steel-fiber-reinforced cementitious composites. *Journal of Composite Materials*, 49(29):3621–3634.

[11] Aydın, S., Baradan, B. (2013). The effect of fiber properties on high performance alkali-activated slag/silica fume mortars. *Composites Part B: Engineering*, 45(1):63–69.

[12] Nguyen, D.-L., Nguyen, T.-Q., Nguyen, H.-T.-T. (2020). Influence of fiber size on mechanical properties of strain-hardening fiber-reinforced concrete. *Journal of Science and Technology in Civil Engineering (STCE) - NUCE*, 14(3):84–95.

[13] Hannawi, K., Bian, H., Prince-Agbodjan, W., Raghavan, B. (2016). Effect of different types of fibers on the microstructure and the mechanical behavior of Ultra-High Performance Fiber-Reinforced Concretes. *Composites Part B: Engineering*, 86:214–220.

[14] ACI PRC-544.4-18 (2018). *Guide to Design with Fiber-Reinforced Concrete*.

[15] Naaman, A. E. (2004). Strain hardening and deflection hardening fiber reinforced cement composite. In *Proceedings of the Fourth International Workshop on High Performance Fiber Reinforced Cement Composites (HPFRCC4)*, 95–113.

[16] Kim, J. J., Kim, D. J., Kang, S. T., Lee, J. H. (2012). Influence of sand to coarse aggregate ratio on the interfacial bond strength of steel fibers in concrete for nuclear power plant. *Nuclear Engineering and Design*, 252:1–10.

[17] Choi, M., Kang, S.-T., Lee, B., Koh, K.-T., Ryu, G.-S. (2016). Improvement in Predicting the Post-Cracking Tensile Behavior of Ultra-High Performance Cementitious Composites Based on Fiber Orientation Distribution. *Materials*, 9(10):829.

[18] Tran, N. T., Kim, D. J. (2017). Synergistic response of blending fibers in ultra-high-performance concrete under high rate tensile loads. *Cement and Concrete Composites*, 78:132–145.

[19] Nguyen, D.-L., Thai, D.-K., Nguyen, H. T. T., Nguyen, T.-Q., Le-Trung, K. (2021). Responses of composite beams with high-performance fiber-reinforced concrete. *Construction and Building Materials*, 270: 121814.

[20] Kim, D. J., Park, S. H., Ryu, G. S., Koh, K. T. (2011). Comparative flexural behavior of Hybrid Ultra High Performance Fiber Reinforced Concrete with different macro fibers. *Construction and Building Materials*, 25(11):4144–4155.

[21] Ngo, T. T., Kim, D. J. (2018). Synergy in shear response of ultra-high-performance hybrid-fiber-reinforced concrete at high strain rates. *Composite Structures*, 195:276–287.

[22] Naaman, A. E., Reinhardt H., W. (1996). Characterization of high performance fiber reinforced cement composites. In *Proceedings of 2nd international workshop on HPFRCC, Chapter 41, RILEM, No. 31, E.& FNSpon, London*, 1–24.

[23] Naaman, A. E. (1972). A Statistical Theory of Strength for Fiber Reinforced Concrete. PhD thesis, Massachusetts Institute of Technology.

[24] Naaman, A. E. (1987). *High Performance Fiber Reinforced Cement Composites*. Concrete Structures for the future, IABSE Symposium, Paris, France, 371–376.

[25] Naaman, A. E. (2000). *Ferrocement and Laminated Cementitious Composites*. Techno Press 3000, P.O. Box 131038, Ann Arbor, MI 48105, USA.

[26] Park, S. H., Ryu, G. S., Koh, K. T., Kim, D. J. (2014). Effect of shrinkage reducing agent on pullout resistance of high-strength steel fibers embedded in ultra-high-performance concrete. *Cement and Concrete Composites*, 49:59–69.

[27] Yoo, D.-Y., Park, J.-J., Kim, S.-W. (2017). Fiber pullout behavior of HPFRCC: Effects of matrix strength and fiber type. *Composite Structures*, 174:263–276.